Eur. Phys. J. D **8**, 111–116 (2000)

**THE EUROPEAN PHYSICAL JOURNAL D**

EDP Sciences


# Relevance of temporal coherence in the second-harmonic cross-correlation measurement of a multiply scattered laser pulse

A. Andreoni[1,a], M. Bondani[1], M.A.C. Potenza[1], and F. Villani[2]

[1] Dipartimento di Scienze Chimiche, Fisiche e Matematiche, Universita' dell'Insubria, via Lucini, 3, 22100 Como, Italy
and
Istituto Nazionale di Fisica della Materia, I.N.F.M., Milano-Universita', 20133 Milano, Italy
[2] I.N.F.M., Napoli-Universita' Federico II, 80131 Napoli, Italy

Received 7 May 1999

**Abstract.** Second-harmonic cross-correlation operates a selection in time-phase among the randomly dephased contributions to an optical field that propagated through a scattering medium. It can thus be used to selectively detect the weak contribution remaining coherent with the incident field.

**PACS.** 42.65.Ky Harmonic generation, frequency conversion – 42.25.Kb Coherence – 42.25.Dd Wave propagation in random media

## 1 Introduction

Since years, non-linear optical interactions have been exploited in cross-correlation techniques for obtaining images or, at least, detecting the presence of objects immersed in turbid media, when the objects were transilluminated by intense laser pulses. Only recently, however, has attention been brought to the advantages that the coherence of these interactions may bring about to distinguish the weak image-bearing field contribution from the overwhelming randomly scattered field [1,2]. In general, this selection is operated either in time or in propagation direction, due to the fact that a feature of the field to be detected is that it has not taken random paths while propagating after the object. Non-linear optical interactions, occurring in both $\chi^{(2)}$ and $\chi^{(3)}$ media, are suitable for operating either selection: time gating is performed by cross-correlating the field behind the object with optically delayed replicas of the incident field (reference field), whereas space Fourier filtering is obtained through the fulfilment of the phase-matching condition required for generating the cross-correlated signal.

The general property that a non-linear interaction couples only fields whose temporal phases are linked to each other is rather relevant in both cases. It implies, for instance, that with a broadband pulse, that is a non transform-limited pulse, a time gate can be generated of duration much shorter than the pulse duration: the temporal width of the gate is rather of the order of the inverse pulse bandwidth. By using this fact, Bashkansky *et al.* [3] were able to generate a coherently amplified Raman polarisation (CARP) gate as short as 335 fs by using a 8-ns dye-laser pulse of $6 \times 10^{12}$ Hz bandwidth. We recently showed that, with second-harmonic (SH) cross-correlation, one can selectively up-convert only those components of the field travelling in the forward direction behind the object that are in phase with those of the reference field [2]. Since these are the components carrying image information, we could obtain clean far-field diffraction patterns of a 1D object by using a 18-ns Nd:YAG-laser pulse to transilluminate it: time gating was demonstrated to be not necessary, if the field sent to the up-converting crystal was the one leaving the object in a relatively narrow angle about the forward direction [2,4].

In either CARP or SH cross-correlation experiments aimed at detecting objects through scattering media [1,2,4], obvious advantages, both technical and economical, arise from the possibility of using $Q$-switched instead of femtosecond lasers with chirp-pulse amplifiers and compressors. When medical imaging is considered, an important further advantage is that higher intensities can be used, since the maximum allowed energy fluences are higher, if nanosecond instead of picosecond pulses are shed onto human tissues [5]. This is particularly relevant for CARP cross-correlation, which allows a 2D resolution suitable for the diagnosis of embedded tissue abnormalities [6], because stimulated Raman scattering amplification does not require phase matching.

## 2 Experimental set-up

The scheme we adopted in our experiments of SH cross-correlation is the same as that reported in [2]. We used a $\beta$-barium-borate crystal in type I phase-matching (BBO I,

[a] e-mail: andreoni@fis.unico.it

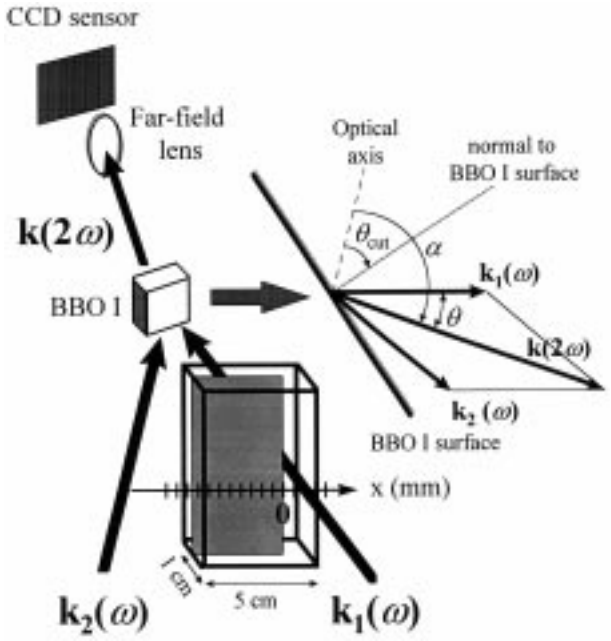


**Fig. 1.** Experimental set-up for measurements of SH cross-correlated far-field patterns and geometry of the interaction inside the BBO I crystal.

thickness: 2-mm, cross-sectional area: $5\times5$ mm$^2$), in which the wave-vectors of the fields to be cross-correlated, $\mathbf{k}_1(\omega)$ and $\mathbf{k}_2(\omega)$ in Figure 1, cross at an angle $2\vartheta$ to each other. Thus, at difference with CARP gating systems, our system is endowed with 1D resolution along a direction in the horizontal plane, which is also the incidence and the tuning plane (tuning angle, $\alpha$), as depicted in Figure 1. In this paper, we show that the coherence of the three-wave interaction used for frequency up-conversion is responsible not only for the selective conversion of the fraction of field not affected by the scattering, but also for the space resolution of the technique. We think that the experimental results and their theoretical interpretation here reported add value to the fact that a $Q$-switched laser is used, in that our technique of coherent phase-sensitive detection opens the possibility of developing portable object-finders with relatively long ranges.

All experiments were carried on with the non-amplified output of a $Q$-switched Nd:YAG laser (mod. Quanta-Ray GCR-4, Spectra-Physics Inc., Mountain View, CA), with 18-ns pulse duration, $\sim 1$ cm$^{-1}$ bandwidth. The output beam was spatially filtered to achieve a beam quality similar to that of a diffraction-limited beam, according to the divergence measured over $\sim 4$ m propagation in air. The fundamental Nd laser pulses were 50% split into two pulses, one sent to the sample and the other used as the reference, arriving coincident in time at the BBO I crystal. At the entrance of the sample cell, a $1\times5$ cm$^2$ quartz cuvette (optical path: 1 cm) partially blanked by a stainless steel blade with a very sharp and straight vertical edge and filled with a turbid medium (see Fig. 1 and [2]), the beam cross-section was 870 $\mu$m in full-width at half maximum (FWHM) diameter and the incident intensity, averaged across the spot, was 11.5 MW/cm$^2$. Far-field intensity distributions were measured both for beam 1 at the wavelength of 1.064 $\mu$m, as collected by the lens shown in Figure 1 in an angle $\psi$ around $\mathbf{k}_1(\omega)$, and for its frequency-doubled replica. The latter, with wave-vectors $\mathbf{k}(2\omega)$, was obtained upon cross-correlation to the reference field travelling along $\mathbf{k}_2(\omega)$ according to the geometry sketched in Figure 1, which was characterised by the angles $\vartheta = 2.86°$ and $\alpha = 23.4°$ inside the BBO I crystal ($\vartheta_{\rm cut} = 40°$). Micelle suspensions of Intralipid (Pharmacia, Italy) in doubly-distilled water constituted the turbid media. Note that the volume-to-volume concentrations of Intralipid quoted in this paper are absolute percent values that include the 10% dilution factor of the commercial product [7]. Prior to each experiment, once established the angle between beams 1 and 2, the sample cell was filled with water and the crystal tuned in angle for maximum SH cross-correlation. The focal plane of the light collecting lens (nominal $f$: 15 cm, diameter: 2 cm) was made to coincide with the sensor plane of the CCD camera. The camera, which was alternatively used to detect either the up-converted or the fundamental (beam 1) far-field intensity distribution, was a Pulnix (mod. PE2015, Pulnix Europe, Basingstoke, UK) and was connected to a Spiricon (mod. LBA100, Spiricon, Logan, UT) for image analysis. Suitable neutral-density filters with calibrated optical densities were put before the CCD camera in each measurement in order to ensure a linear response of the detecting/digitising apparatus. When up-converted signals were to be measured, a band pass filter was added to cut the stray light at the fundamental wavelength.

## 3 Results and discussion

We first report on experiments in which the cell was filled with 0.67% Intralipid, which gives a collimated transmittance through the sample of $\sim 1.15\times10^{-4}$ at 1.064 $\mu$m. In these experiments, the cell was shifted in the $x$ direction (see Fig. 1) and the measurements were repeated for different distances, $x$, of beam centre to blade edge (for $x<0$, beam 1 strikes the blank). Field 1 contributions travelling at angles $\psi \leq 20.8$ mrad to $\mathbf{k}_1(\omega)$ were accepted by both the far-field lens, in the measurements at $\omega$, and the BBO I crystal, in those at $2\omega$. Integrals (*i.e.* power) and peak values (*i.e.* maximum intensity, as power $\times$ (mrad)$^{-2}$) of the far-field patterns, as obtained from the mapped intensity values, are plotted in Figure 2. The filled symbols refer to the measurements at $\omega$ and the open symbols to those at $2\omega$. The latter ones are only reported for $x = +2.75$ mm, because SH cross-correlation did not give detectable signals at $x \leq -1.02$ mm. On the contrary, infrared scattered light evidently enters the collection angle $\psi$ of the lens even when the incident-beam spot falls onto the opposite side of the blade, more than 4 mm away from the edge. Note that, as long as the tails of the intensity distributions are not cut by the low-limit sensitivity of the CCD, the curves of integrals and peak values run parallel to each other on the logarithmic scale of Figure 2. Since the ratio of integrals to peak values is a measure of the detected spot

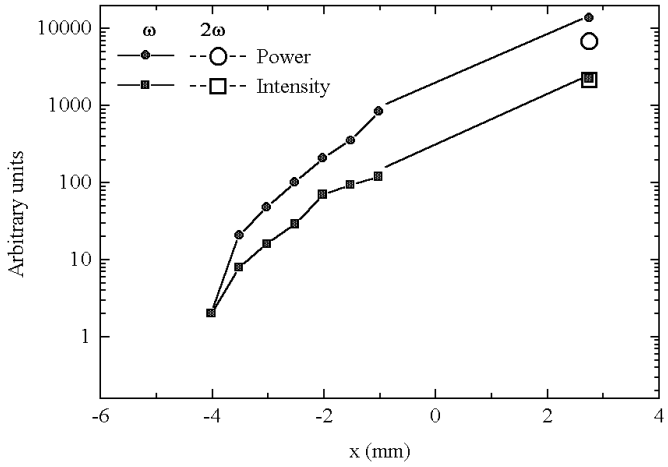


**Fig. 2.** Power and peak intensity values of the far-field patterns recorded when the beam is shed at distance $x$ from the edge of the blank immersed in the cell filled with 0.67% Intralipid. The intensity is expressed in the same units as the power (a.u.) divided by $(\text{mrad})^2$.

area in $(\text{mrad})^2$, we can assess that the scattered field 1 that gets around the obstacle has a far-field intensity distribution similar in shape to that of the beam allowed to pass through the medium. This scattered field, however, does not produce detectable up-converted signal. In order to achieve a detectable SH cross-correlated signal level in the case of blanked beam in 0.67% Intralipid, we then increased the acceptance angle $\psi$ ($\psi = 80$ mrad, $\vartheta = 3.33°$ and $\alpha = 23.6°$, incident intensity and incident spot diameter as above) and made measurements for $x = -0.25$ mm (see 3D plots in Figs. 3a and 3b) and $x = +0.25$ mm (see Fig. 3c). In the former case, though the obstacle just stops the most intense part of the beam cross-section, the SH cross-correlated far-field pattern shown in Figure 3b is a noisy one, with no memory of the scattered field pattern as measured at $\omega$ and reported in Figure 3a. On the contrary, a narrow pattern is obtained when SH cross-correlation is performed for $x = +0.25$ mm, as shown in Figure 3c.

It might be argued that the cross-correlated signal vanishes as soon as the incident spot takes the blank because of the corresponding strong decrease in intensity at $\omega$ (see the high level of noise in Fig. 3a and the slope of the plots in Fig. 2 on going toward negative $x$ values). We think that the next experiment rules out this possibility. We compared the far-field distributions, at both $\omega$ and $2\omega$, for the field transmitted through the scattering medium (position: $x = +2.75$ mm, see data in Fig. 2) with those for the field transmitted through the cuvette filled with water. All other experimental conditions were as in the first experiment. The results are displayed in the maps in Figure 4, where the FWHM levels are highlighted. The comparison of the measurement at $\omega$ with that at $2\omega$ for field 1 transmitted by water, in Figures 4a and 4a', respectively, shows that the non-linearity of the cross-correlation has only little effect on the FWHM of the detected far-field intensity pattern, in that the FWHM angular spread of the $\mathbf{k}_1(\omega)$ wave-vectors, 0.37 mrad, produces a FWHM value

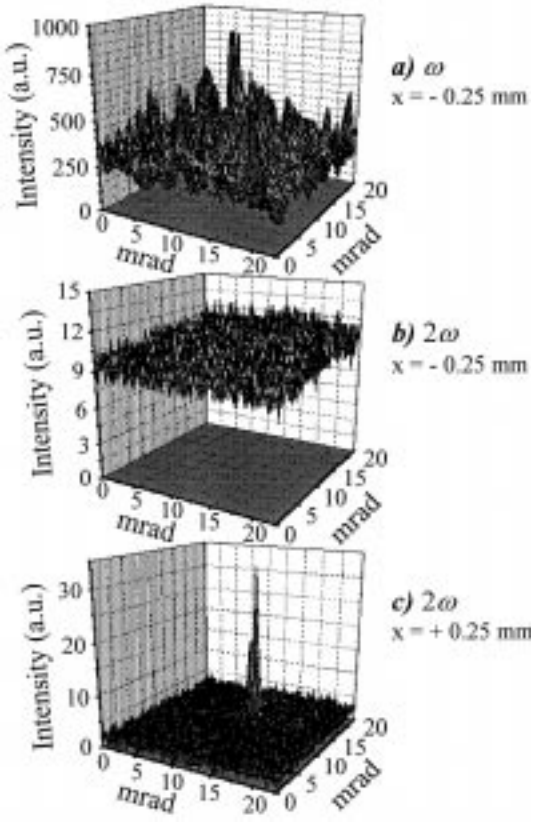


**Fig. 3.** Far-field intensity distributions of a 870 $\mu$m diameter beam either striking onto the blank or passing through 1 cm of 0.67% Intralipid.

of 0.36 mrad for the wave-vectors $\mathbf{k}(2\omega)$ upon SH cross-correlation. By contrast, the pattern at $\omega$ after the scattering medium, with FWHM value of 0.48 mrad (Fig. 4b), which is markedly broader than that transmitted by water (see Fig. 4a), results in a $\mathbf{k}(2\omega)$ pattern as narrow as that of the cross-correlated scattering-free field 1 (see Figs. 4b' and 4a'). We conclude that relatively low and similar intensity levels at $\omega$ are frequency up-converted with lower efficiency when the field is transmitted by a scattering medium rather than by a non-scattering medium.

At last, the lack of up-conversion of the wings in Figure 4b might originate from a phase mismatch, which increases on going from the peak to the edge of the far-field pattern that exceeds the non-linear interaction bandwidth. In the following theoretical treatment, we demonstrate that the bandwidth of SH conversion is by far sufficiently broad to allow up-conversion of the most diverging $\mathbf{k}_1(\omega)$ wave-vectors recorded in the scattered field at $\omega$ in Figure 4b. Further experimental support to this statement is provided by the results in [2,4], where we reported efficient conversion for diffraction maxima of a narrow-needle that extended over even greater angles.

The space-dependent fields, two of which, at frequencies $\omega_1$ and $\omega_2$, propagate at the angles $\vartheta_1$ and $\vartheta_2$ on opposite sides respect to the phase-matched wave-vector

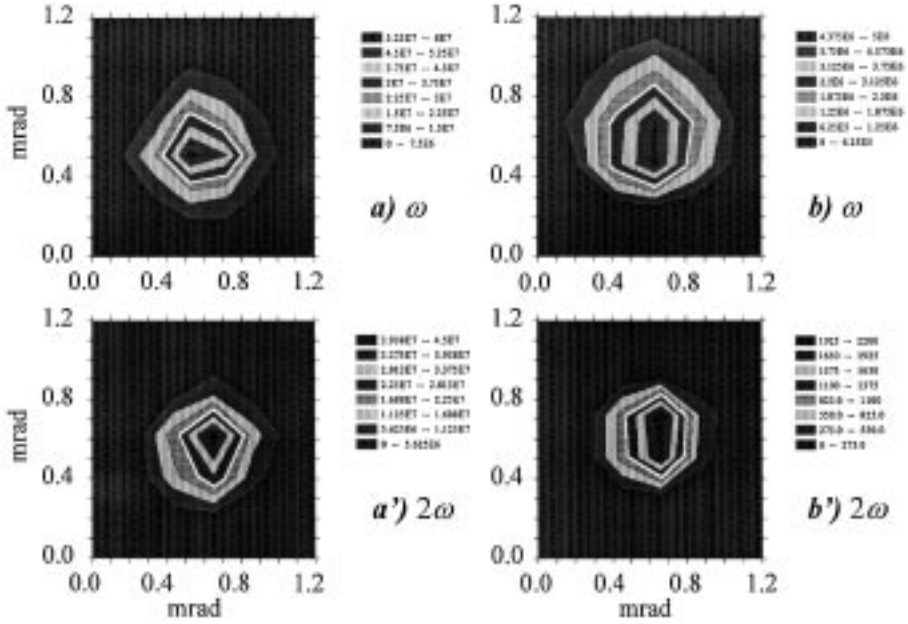


**Fig. 4.** Far-field intensity distributions of a 870 $\mu$m diameter beam passing through 1 cm of either water (a and a') or 0.67% Intralipid (b and b'). The 50% level is highlighted by white lines.

$\mathbf{k}_3(\omega_3 = \omega_1 + \omega_2)$, can be written as:

$$\mathbf{E}_1(y,z) = \frac{1}{2}\sqrt{2\eta_1\hbar\omega_1}\,[a_1(z)\exp(-\mathrm{j}k_1\cos\vartheta_1 z - \mathrm{j}k_1\sin\vartheta_1 y) + c.c.]\,\hat{\mathbf{x}} \tag{1a}$$

$$\mathbf{E}_2(y,z) = \frac{1}{2}\sqrt{2\eta_2\hbar\omega_2}\,[a_2(z)\exp(-\mathrm{j}k_2\cos\vartheta_2 z - \mathrm{j}k_2\sin\vartheta_2 y) + c.c.]\,\hat{\mathbf{x}} \tag{1b}$$

$$\mathbf{E}_3(y,z) = \frac{1}{2}\sqrt{2\eta_3\hbar\omega_3}\,\{[a_{3y}(y,z)\hat{\mathbf{y}} + a_{3z}(y,z)\hat{\mathbf{z}}]\exp(-\mathrm{j}k_3 z) + c.c.\} \tag{1c}$$

being $\mathbf{k}_3(\omega_3)$ along the $z$-axis. In equations (1a, 1b, 1c), $\eta_{1,2,3} = (\mu_0/\varepsilon_0)^{1/2}/n_{1,2,3}$ and $k_{1,2,3} = n_{1,2,3}\omega_{1,2,3}/c_0$, being $\mu_0$ and $\varepsilon_0$ the magnetic permeability and electric permittivity, $n_{1,2,3}$ the refractive indices and $c_0$ the speed of light in the vacuum. In the case $a_2(z) \cong a_2(0)$, which occurs in our experiments since the reference pulse is not depleted by the interaction, the fields in equations (1a, 1b, 1c) can be calculated. In particular, by imposing also the boundary condition $a_{3y}(y,0) = a_{3z}(y,0) = 0$, we find:

$$|a_3(y,z)|^2 = a_{3y}^2(y,z) + a_{3z}^2(y,z) = |g a_1(0) a_2(0)|^2 z^2 \mathrm{sinc}^2\left(\frac{z}{2}\sqrt{\Delta k_\parallel^2 + 4\cos\vartheta_1 g^2 |a_2(0)|^2}\right). \tag{2}$$

In equation (2), $g$ is given by:

$$g = \sqrt{2\hbar\eta_0^3 \frac{\omega_1\omega_2\omega_3}{n_1 n_2 n_3}(d_{22}^2 + d_{31}^2)} \tag{3}$$

being $d_{ij}$ the elements of the second-order susceptibility tensor, and

$$\Delta k_\parallel = k_3 - k_1\cos\vartheta_1 - k_2\cos\vartheta_2 \tag{4}$$

represents the phase mismatch in the $z$ direction. In the case of SH cross-correlation of fields 1 and 2 in a BBO I crystal, the photon conversion efficiency, $\varepsilon$, defined as $\varepsilon = \varepsilon(z) = |a_3(z)|^2/|a_1(0)|^2$, turns out to be:

$$\varepsilon(z) = \gamma^2 \frac{\sin^2\left(\sqrt{\Delta k_\parallel^2 + \gamma^2\cos\vartheta}\,\frac{z}{2}\right)}{\Delta k_\parallel^2 + \gamma^2\cos\vartheta} \tag{5}$$

where $\gamma^2$ is given by:

$$\gamma^2 = 16(d_{22}^2 + d_{31}^2)\eta_0^3 \frac{\omega^2}{n_{\mathrm{F}}^2 n_{\mathrm{SH}}(\alpha)} I \tag{6}$$

and $n_{\mathrm{F}}$ and $n_{\mathrm{SH}}(\alpha)$ are the refractive indices experienced by fundamental and up-converted fields and $I$ denotes the incident intensity of the reference beam 2. Upon substitutions with the numerical values ($d_{22} = 17.7 \times 10^{-24}$ C$^3$/J, $d_{31} = 1.24 \times 10^{-24}$ C$^3$/J, averages of literature data [8], $\alpha = 23.4°$, $I = 11.5$ MW/cm$^2$), equation (6) gives $\gamma^2 \cong 15\,351$ m$^{-2}$ for the experiment in Figure 4. Thus, the photon conversion efficiency at the crystal exit, $\varepsilon(L = 2\text{ mm})$, can be calculated from equation (5) with $\vartheta = 2.86°$. A $z$ value equal to the crystal depth $L$ has been taken, because both SH walk-off and the difference between $\alpha$ and $\vartheta_{\mathrm{cut}}$ were disregarded. In our conditions, the photon-conversion efficiency turns out to achieve a maximum value of $\sim$ 1.53% for $\Delta k_\parallel = 0$ and to drop to zero for $\Delta k_\parallel \cong 32$ cm$^{-1}$. Since, in phase matching, we have $k_1\cos\vartheta \cong 48\,791$ cm$^{-1}$, in order to achieve a mismatch

of $\pm 16$ cm$^{-1}$ the $\mathbf{k}_1$ wave-vector should deviate from $\vartheta$ by as much as $\sim +6.2$ mrad and $\sim -7.1$ mrad (on opposite sides). Such deviations are much greater than the overall angular spread of the far-field pattern at $\omega$ in Figure 4b, which only covers $\pm 0.24$ mrad about the peak. Therefore the entire pattern of the scattered wave-vectors should be up-converted.

As in our previous work [2], we are forced to conclude that SH cross-correlation reduces the contributions of the incoherent field in the detected far-field patterns because it is a coherent effect. Let us consider the part of field 1 propagating in a direction along which some ballistic signal travels. This means that we take the overall, coherent and incoherent, field 1 having wave-vector equal to that of the incident field, $\mathbf{k}_1(\omega)$ in Figure 1. The effect of the turbid medium on a frequency component at $\omega$ of the incident field:

$$\mathsf{E}_1(t) = \mathbf{E}_1 \mathrm{e}^{\mathrm{j}\omega t} \tag{7}$$

is to split it into $N$ incoherent fields

$$\mathsf{E}_{1,\phi}(t) = \mathbf{E}_{1,\phi} \mathrm{e}^{\mathrm{j}(\omega t - \phi)} \tag{8}$$

plus a single one, coherent with the incident component, $\mathsf{E}_{1,0}(t)$, that is still a fraction of the field in equation (7):

$$\mathsf{E}_{1,0}(t) = \mathbf{E}_{1,0} \mathrm{e}^{\mathrm{j}\omega t}. \tag{7'}$$

Note that, in the absence of absorption losses by the medium, the only restriction on the amplitudes is that the overall intensity at $\omega$ carried, out of the sample, by all fields $\mathsf{E}_{1,\phi}(t)$ and by the coherent one $\mathsf{E}_{1,0}(t)$ is given by $|\mathbf{E}_1|^2$. In addition, the $N$ de-phasing angles, $\phi$ in equation (8), have any value in the interval $(-\pi, +\pi)$. According to equation (1a) and in the simple case of collinearly propagating fields, we can write the space-dependent complex amplitude $E_{1,0} = E_{1,0}(z)$ of the coherent field in equation (7') after travelling a $z$ optical pathway inside the BBO I crystal, as

$$E_{1,0}(z) = \sqrt{2\eta_{\mathrm{F}}\hbar\omega}\, a_1(z) \mathrm{e}^{-\mathrm{j}k_1 z} \tag{9}$$

where $\eta_{\mathrm{F}} = (\mu_0/\varepsilon_0)^{1/2}/n_{\mathrm{F}}$. If we define

$$a'_{1,\phi}(z) = a_{1,\phi}(z) \mathrm{e}^{-\mathrm{j}\phi} \tag{10}$$

also the space-dependent complex amplitude, $E_{1,\phi} = E_{1,\phi}(z)$, of any incoherent component in equation (8) can be re-written as

$$E_{1,\phi}(z) = \sqrt{2\eta_{\mathrm{F}}\hbar\omega}\, a'_{1,\phi}(z) \mathrm{e}^{-\mathrm{j}k_1 z}. \tag{9'}$$

Since equation (9') is identical to equation (9), upon substituting $a_1(z)$ with $a'_{1,\phi}(z)$, the equations coupling $a'_{1,\phi}(z)$ to the complex amplitudes of field 2, $a_2(z)$, and of the field at $2\omega$, $a_3(z)$, which are defined according to equations (1b, 1c) for $\vartheta_1 = \vartheta_2 = 0$, are those that apply to $a_1(z)$, $a_2(z)$, and $a_3(z)$ [9]. These equations can be solved in the approximation $a_2(z) \cong a_2(0)$ and give, when $\Delta k = k_3 - k_1 - k_2 = 0$,

$$a_{3,\phi}(z) = -\mathrm{j} a'_{1,\phi}(0) \sin\frac{\gamma z}{2} \tag{11}$$

or, by substituting equation (10),

$$a_{3,\phi}(z) = -\mathrm{j} a_{1,\phi}(0) \mathrm{e}^{-\mathrm{j}\phi} \sin\frac{\gamma z}{2} \tag{11'}$$

with $\gamma = 2g a_2(0)$. Note that, to get the solution in equation (11), we assumed the coupling equations for collinearly propagating fields as valid, but disregarded the field at $2\omega$ generated by the autocorrelation of either fields 1 or 2 because these interactions are phase-mismatched in our non-collinear phase-matching geometry.

Since scattering is a random phenomenon, there is no reason to support any peculiar behaviour of $a_{1,\phi}(0)$ as a function of $\phi$. If one takes into account that (i) all fields that propagated in the turbid medium for pathlengths, $d$, differing from each other by multiples of $\lambda_{\mathrm{F}}(d_n = d \pm n\lambda)$ contribute to the amplitude $a_{1,\phi}(0)$ with $\phi = (2\pi/\lambda)d$ and that (ii) the probability distribution for the pathlength, $P(d)$, exhibits significant variations only over intervals $\Delta d \gg \lambda_{\mathrm{F}}$, it seems reasonable to assume that the amplitudes $a_{1,\phi}(0) \propto \sum_n P(d_n)$ are virtually independent of $\phi$. For such equal incoherent amplitudes, equation (11') leads to equal-amplitude incoherent contributions to the up-converted field 3. Their sum (vector sum in the complex plane) is thus proportional to $\sqrt{N}\langle a_{1,\phi}(0)\rangle$ in magnitude and has a phase value $\Phi - \pi/2$, where $\Phi$ denotes the phase of the overall scattered field 1 as given by the random-walk statistics. The corresponding field at $2\omega$ (see Eq. (1c)) should then be added to the one generated by the coupling of field 2 with the coherent field $\mathsf{E}_{1,0}$, described by equations (7', 9), and an overall field with space-dependent complex amplitude

$$E_3(z) = \sqrt{4\eta_{\mathrm{SH}}\hbar\omega}\left\{-\mathrm{j}\left[a_1(0) + \sqrt{N}\langle a_{1,\phi}(0)\rangle \mathrm{e}^{-\mathrm{j}\phi}\right]\sin\frac{\gamma z}{2}\right\}\mathrm{e}^{-\mathrm{j}k_3 z} \tag{12}$$

would be obtained at $2\omega$, with $\eta_{\mathrm{SH}} = (\mu_0/\varepsilon_0)^{1/2}/n_{\mathrm{SH}}$. Thus, in the $E_3(z)$ amplitude, the signal to noise (*i.e.* coherent to incoherent) ratio is $a_1(0)/(\sqrt{N}\langle a_{1,\phi}(0)\rangle)$, that is the same as that in the $E_1(0)$ amplitude.

Due to the bandwidths of both laser pulse and photon-conversion efficiency, the interaction $\mathbf{k}_1(\omega)$, $\mathbf{k}_2(\omega) \rightarrow \mathbf{k}(2\omega)$ is not the only one producing field at $2\omega$ according to equation (12). Other contributions arise from the interactions $[\mathbf{k}_1(\omega \pm \Delta\omega), \mathbf{k}_2(\omega \mp \Delta\omega)] \rightarrow \mathbf{k}(2\omega)$ for all $\Delta\omega$ values within the bandwidth. Note that, in our case, the relevant bandwidth is the one of the laser pulse, which is narrower than that of the SH interaction. To decide how these contributions modify the signal to noise ratio in the overall $E_3(z)$ amplitude, it is convenient to re-write

equation (12) as

$$E_3(z) \cong \sqrt{4\eta_{\rm SH}\hbar\omega}\left\{-\mathrm{j}\left[a_1(0)+\sqrt{N}\langle a_{1,\phi}(0)\rangle \mathrm{e}^{-\mathrm{j}\Phi}\right]a_2(0)\right\} g z e^{-\mathrm{j}k_3 z} \quad (12')$$

and to take into account that $a_1(0)$, $a_{1,\phi}(0)$ and $a_2(0)$ now refer to frequencies shifted by $\pm\Delta\omega$ with respect to the central laser frequency $\omega$. If the incident pulse spectrum contains $M$ frequencies with relevant amplitudes, say, the $M$ longitudinal modes of the Nd:YAG laser, the term $a_1(0)a_2(0)$ in equation (12') obtained for field 1 at $\omega+\Delta\omega$ and field 2 at $\omega-\Delta\omega$ has the same phase as that of the term obtained for field 1 at $\omega-\Delta\omega$ and field 2 at $\omega+\Delta\omega$, independently of the time-coherence properties of the pulse. Therefore, in the calculation of the overall amplitude at $2\omega$, these two terms add coherently and produce a contribution, $C_{\pm\Delta\omega}$, proportional to $2a_1(0)a_2(0)$. By assuming, for simplicity, a flat spectral profile, the integral contribution for all $\Delta\omega$ values will have an amplitude proportional to either $(M/2)C_{\pm\Delta\omega}$ or $\sqrt{M/2}C_{\pm\Delta\omega}$ for a transform-limited or a non-transform-limited incident pulse, respectively. By contrast, and independently of the coherence properties of the incident pulse, the second term in equation (12') originates $M$ randomly de-phased contributions at the different $\Delta\omega$ values, whose sum will have an amplitude proportional to $\sqrt{MN}a_1(0)a_2(0)$. In conclusion, the overall result of the interactions $[\mathbf{k}_1(\omega\pm\Delta\omega),\ \mathbf{k}_2(\omega\mp\Delta\omega)] \rightarrow \mathbf{k}(2\omega)$ is an increase in the ratio of coherent to incoherent contributions in the $E_3(z)$ amplitude, with respect to the ratio, $\approx 1/\sqrt{N}$, obtained in the case of monochromatic interaction (see above). In fact, the ratio becomes a number between $\sqrt{2/N}$ and $\sqrt{M/N}$, depending on the coherence of the incident (and reference) pulse. For a given bandwidth of the incident pulse, *i.e.* for a given $M$ value ($M\cong 100$ in our case), a field $E_1(0)$ with a coherent to incoherent ratio proportional to $1/\sqrt{N}$ is then up-converted into a field $E_3(z)$ in which this ratio is enhanced by a factor that can be as great as $\sqrt{M}$, if the $M$ modes are linked in phase, but cannot be smaller than $\sqrt{2}$. The coherence of the SH cross-correlation is entirely responsible for these results, including the existence of the lower limit, $\sqrt{2}$, which is achieved for fully incoherent laser modes.

The experimental results in Figures 3 and 4 agree with the evaluations of above. The signal to noise ratio in Figure 4b has to be taken as proportional to $1/\sqrt{N}$, whereas the signal to noise ratio, $S/N$, in Figure 4b' is the one expected to fall between $\sqrt{2/N}$ and $\sqrt{M/N}$. Though it cannot be appreciated in the plotted intensity maps, $S/N$ is greater by a factor $R\cong 25$ in Figure 4b' as compared with Figure 4b. Note that a purely scattered field, such as that measured in Figures 3a and 3b gives detected signals that are in a similar ratio to each other, when detected at $\omega$ (Fig. 3a) rather than upon SH cross-correlation, as in Figure 3b. According to the considerations of above, the coherent-to-incoherent field detectability ratio, $\sqrt{R}$, should be comprised in the interval $(\sqrt{2},\ \sqrt{M})$.

In conclusion, we showed that SH cross-correlation with the incident field of the forward-scattered field is a means to detect the low-intensity residual coherent field immersed in the scattered incoherent one, even when the latter is more intense. The cross-correlation selectivity for the coherent field seems to result predominantly from the coherence rather than the spatial-filtering action of the non-linear interaction.

M.A.C. Potenza acknowledges E.N.E.A. (Ente per le Nuove tecnologie, l'Energia e l'Ambiente) for his Ph.D. studentship. All authors are deeply indebted with F. Ferri (University of Insubria) for the useful comments and suggestions. This work was supported in part by the Italian National Research Council (C.N.R.) through grants 96.00264.CT02 and 97.00070.CT02.

## References

1. M. Bashkansky, J. Reintjes, Opt. Lett. **18**, 2132 (1993).
2. A. Andreoni, M. Bondani, M.A.C. Potenza, F. Villani, J. Nonlin. Opt. Mat. **8**, 55 (1999).
3. M. Bashkansky, C.L. Adler, J. Reintjes, Opt. Lett. **19**, 350 (1994).
4. A. Andreoni, M. Bondani, M.A.C. Potenza, A. Lukashev, F. Villani, in *Proceedings of Nonlinear Optics'98, Materials, Fundamentals and Applications Topical Meeting, Princeville, Kauai, Hawaii, 1998* (IEEE, catalog #98CH36244, Piscataway, NJ, 1998), p. 432.
5. D. Sliney, M. Wolbarsht, *Safety with Lasers and Other Optical Sources* (Plenum, New York, 1982), pp. 261-283.
6. J.A. Moon, P.R. Battle, M. Bashkansky, R. Mahon, M.D. Duncan, J. Reintjes, Phys. Rev. E **53**, 1142 (1996).
7. H.J. van Staveren, C.J.M. Moes, J. van Marle, S.A. Prahl, M.J.C. van Gemert, Appl. Opt. **30**, 4507 (1991).
8. V.G. Dmitriev, G.G. Gurzadyan, D.N. Nikogosyan, *Handbook of Nonlinear Optical Crystals* (Springer-Verlag, Berlin, Heidelberg, 1991).
9. B.E.A. Saleh, M.C. Teich, *Fundamentals of Photonics* (John Wiley & Sons, New York, 1991), pp. 762-771.